Int. J. Electrochem. Sci., 8 **(2013)** 149 - 158

International Journal of
ELECTROCHEMICAL
SCIENCE
www.electrochemsci.org

Graphene Supported Pt-Co Alloy Nanoparticles as Cathode Catalyst for Microbial Fuel Cells

Zhenhua Yan[1], *Min Wang*[1,2], *Baoxu Huang*[3], *Renmin Liu*[1,*], *Jinsheng Zhao*[1,*]

[1] Shandong Key Laboratory of Chemical Energy-storage and Novel Cell Technology, Liaocheng University, 252059, Liaocheng, P.R. China
[2] The Central Laboratory of Liaocheng Hospital, 252000 Liaocheng, P.R. China
[3] Department of Materials Chemistry, Liaocheng University, 252059, Liaocheng, P.R. China
[*]E-mail: liurenmin@126.com; j.s.zhao@163.com

Received: 13 November 2012 / *Accepted:* 30 November 2012 / *Published:* 1 January 2013

High catalytic activity of Pt-Co/G (15 wt% Pt) alloy particles are synthesized on reduced graphene oxide (RGO) and reduced by simple ethylene glycol (EG). The results of X-ray diffraction and transmission electron microscopy analysis show that the average size of metal particles is ca. 4.1 nm, and the metal particals are highly dispersed on the graphene. The cyclic voltammogram was used for evaluating the electrocatalytic activity of the catalyst. In addition，the performance of this catalyst was investigated in microbial fuel cells (MFCs). It produced a maximum power density of 1378 mW/m^2, which was quite close to that with a Pt/C (20 wt% Pt) cathode (1406 mW/m^2); the Coulombic efficiency reaches 71.6%, which was better than that of the Pt/C (52.0 %). And the total cost of Pt-Co/G catalyst were lower than that of Pt/C catalyst. Thus, the Pt-Co/G probably provides a new solution for finding effective cathode materials for MFC.

Keywords: Graphene; Pt-Co alloy nanoparticles; Microbial full cell; Oxygen reduction reaction; Catalyst.

1. INTRODUCTION

Microbial fuel cells (MFCs) have emerged in recent years as a promising yet challenging technology, known as the environmentally friendly and sustainable power sources, have gained a lot of attention as a mode of converting organic waste including low-strength wastewaters and lignocellulosic biomass into electricity [1]. The Pt-based catalyst is currently one of the key components in fuel cells, which accounts for about 30% of the cost of fuel cell manufacturing [2]. A key challenge to the ultimate commercialization of fuel cells is the development of active, steady, and low-cost catalysts for an oxygen reduction reaction (ORR) [3, 4]. Although considerable progress was

achieved for performance improvement in the last decade [5, 6], the high cost of Pt catalyst and low cathodic oxygen electroreduction activity have still remained as obstacles to overcome. So there has been increasing interest in developing Pt-alloy or alternative catalysts which are low-cost, active, and stable [7, 8]. Considering the activity and stability, platinum-based catalysts are still possess many superiorities for MFCs especially for ORR occurring at the cathode. And recent work on the cathode electrocatalysts has focused on Pt-based bimetallic catalysts such as Pt-Fe, Pt-Ni, Pt-Cr, Pt-Cu, Pt-Au, and Pt-Co, etc.

Carbon black-supported Pt is widely used as an oxygen reduction electrocatalyst for energy conversion device applications. But the vulnerability toward oxidation of carbon black support hinders its use for electrode applications [9]. It is consequently of increasing interest to develop new support materials that avoid the drawbacks linked to carbon black supports. Graphene (G), the first two-dimensional material to be isolated, has become the focus of intense fundamental research due to its extraordinary properties, such as good electronic conductivity, large surface area, high mechanical and/or thermal stability and durability, makes it as a promising catalyst support material for fuel cell applications [10-12]. One encouraging aspect of graphene is to replace carbon black in various applications because the naturally abundant and cheap graphite flakes are used to produce graphene. Since chemical oxidation method has been regarded as the most promising way to produce graphene sheets from both scale and cost perspectives [13]. Thus, intensive effort has focused on using reduced graphene oxide（RGO）as a catalyst support for the ORR, and some exciting results have been reported [14-16]. In comparison with carbon black or carbon nanotubes (CNTs), graphene not only possesses similar physical properties but also larger surface areas. Additionally, production cost of graphene sheets in large quantities is much lower than that of CNTs [12, 17]. It's that believed G close contact with metals play an important role in activity enhancement of the G supported catalyst. This has been demonstrated in the Pt (or Pd)-based nanoparticle catalysts grown on G for electrocatalytic reactions [18-20] and in the activation of Co_3O_4 and MoS_2 NPs by G for oxygen reduction reaction in alkaline media [21] and for hydrogen evolution in H_2SO_4 solution [22]. And also exhibit the advantages of both single-layer graphene and highly graphitic carbon, as a durable alternative support material for Pt nanoparticles for oxygen reduction in fuel cells.

For the purpose of development of low-cost, stable and more active electrocatalysts to replace Pt. In this study we have used RGO as support materials and used EG as reducing agent to fabricate Pt-Co alloy nanoparticles, although these Pt-Co/G (atomic ratio, Pt: Co = 1:1, 15 wt% Pt) alloy catalysts contain reduced content of Pt, they exhibit about the same catalytic activity towards oxygen reduction compared to pure platinum catalyst. Cyclic voltammetry (CV) measurement was used to find out the electrochemical surface area (ECSA) and their electrocatalytic activity for the ORR. X-ray diffraction (XRD) and transmission electron microscopy (TEM) measurements were employed to observe the catalyst structure and size distribution. We also investigated its performance in an air cathode single chamber MFC. For comparison, a commercially available oxygen reduction electrocatalyst of 20 wt% Pt/C was also experimented.

2. EXPERIMENTAL

2.1 Preparation of graphite oxide (GO)

The graphite oxide was synthesized from natural graphite powder (99.99%, 325 mesh) according to the literature [23，24]. After removal of residual salts and acid, the resultant dispersion of graphite oxide was subjected to ultrasonic treatment to obtain the exfoliated GO.

2.2 Preparation of Pt-Co/G alloy catalysts

Pt-Co/G alloy nanoparticles are synthesized by ethylene glycol (Aladdin) reduction method following ref's [25]. In a typical synthesis, stoichiometric amounts of metal precursors $H_2PtCl_6 \cdot 6H_2O$ (Aladdin) as Pt precursor, and $Co(NO_3)_2 \cdot 6H_2O$ (Aladdin) as Co precursor dispersed in 40 ml ethylene glycol solution and 80 mg GO dispersed in 40 ml ethylene glycol solution (ultrasonic treated for an hour in advance) are mixed together with ultrasonic and stirring treatment, 1.0 M NaOH (in EG) was added to adjust the pH of the solution to >13, then the solution was taken in a 250 ml round-bottom flask equipped with a N_2 in/outlet. The resulting suspension is refluxed with vigorously power-driven stirring at 403 K for 7 h. Then it is filtered, washed copiously with ultrapure DI water until Cl^- was not detected and then dried at 333 K in a vacuum oven. The nominal metal content on the graphene is 20 wt.%.

2.3 Electrode preparation

Carbon cloths (3×5 cm) (non-wet proofed, type A, E-TEK) were used as anodes. All the carbon cloths were first cleaned by soaking them in pure acetone (Aladdin) overnight, then acid treated by soaking the cloths in a solution of ammonium peroxydisulfate (200 g/L) and concentrated sulfuric acid (100 mL/L) for 15 min. After that, carbon cloths were heat-treated in a muffle furnace at 450 ºC for 30 min. Following treatments, all cloths were washed three times with distilled water before being used in MFCs. Cathodes were also made of carbon cloth with a projected surface area of 4.5 cm^2; the water proof layer was made as described by previous report [26, 27]: Coated with one layer of a mixture of Vulcan XC-72 (2.5 mg/cm^2) and poly tetrafluoroethylene (PTFE, 60%), and three layers of PTFE (30%) on the air-facing side. The catalytic layer was then prepared as follows: Appropriate amount of Pt-Co/G catalyst (with a Pt loading of 0.375 mg/cm^2), 200 μL of 5 wt% Nafion solution and 100 μL pure iso-propanol were blended in a plastic sample vial, the suspension was coated onto the surface of a carbon cloth. For comparison, cathodes with Pt/C (20 wt%, with a Pt loading of 0.5 mg/cm^2) were prepared using the same method. All electrodes were dried at room temperature for at least 24 h before use.

2.4 MFC construction and operation

Air-cathode single chamber cylindrical MFCs (length 6 cm, diameter 2.4 cm, volume 27 mL) were constructed, and wired to an external resistor (1000 Ω). The cathode was placed on one side of MFC with the oxygen catalyst coating layer facing to the anode, with the PTFE layer exposed directly

to air. The anode was positioned (perpendicularly to the cathode) in the other side of chamber, with a distance of 1.0 cm from the cathode and no membrane between the two electrodes. MFC reactors were inoculated using pre-domesticated bacteria from another double chamber MFC. MFCs were inoculated using solution containing glucose (1 g/L) and a phosphate buffered nutrient medium (PBM) containing NH_4Cl (0.31 g/L), $NaH_2PO_4 \cdot H_2O$ (4.97 g/L), $Na_2HPO_4 \cdot H_2O$ (2.75 g/L), KCl (0.13 g/L), and a metal (12.5 mL) and vitamin (12.5 mL) solution. The solution was replaced at the end of each fed-batch cycle, defined as a voltage less than 50 mV. All tests were conducted in a 35 °C temperature, and were carried out in two parallel samples.

2.5 Analysis and calculation

X-ray diffraction (XRD; D-MAX 2200VPC, RIGAKU) was performed to characterize the catalyst by using Cu Ka radiation. Data acquisition was carried out in the scanning angle range of 10-90°. Diffraction patterns were collected with a scanning rate of 5°per minute and with a step of 0.02°. In order to estimate the particle size from XRD, Scherrer equation was used [28]. For this purpose, the (2 2 0) peak of the Pt around 2-thea=68° was selected. All X-ray diffraction patterns were analyzed using Jade 6.0 software. TEM measurements were carried out on a JEOL-2010; the acceleration voltage was 200 kV. The TEM data were analyzed by Digital Micrograph Demo.

In order to investigate the ORR characterization of the two catalysts, cyclic voltammogram (CV) were performed using an electrochemical work station (CHI 760) with the conventional three-electrode system. A saturated calomel electrode (SCE) and a Pt wire were used as the reference and counter electrode, respectively. The catalysts coated glassy carbon (GC, 3.0 mm diameter) electrodes were used as working electrodes. Homogeneous catalyst ink is prepared by dispersing 5 mg catalyst in 0.125 mL 5 wt.% Nafion solution, 0.125 mL isopropanol and 0.5 mL ultrapure water by sonicating for 30 min, and 3.0 μl of the slurry was deposited on the glassy carbon electrode (area 0.07065 cm^2), then dried at room temperature. After fabrication, the electrodes are immersed in N_2-saturated 0.5 M H_2SO_4 and voltammograms are recorded. All the potential values are given with respect to SCE in the report. The electrochemical surface area (ECSA) of the catalyst was determined by calculating the hydrogen adsorption area. The charge for monolayer adsorption of hydrogen on Pt was assumed to be 210 $\mu C \cdot cm^{-2}$.

The polarization curves and the power density curves were obtained by varying the external resistance (R) from 20000 to 20 Ω, when the voltage output was in steady-state after keep 20000 Ω for an hour, and the voltage (V) changing with the external resistance in the MFC was recorded by a data acquisition system connected to a computer every 10 min. At each resistance (R), MFCs were operated for two batches to ensure repeatable voltage output. The power density (P, mW/m^2) was calculated by the equation 1.

$$P = \frac{V_{cell}^2}{R_{ex} A} \quad (1)$$

and the current density was calculated by equation 2.

$$P = \frac{V_{cell}}{R_{ex} A} \quad (2)$$

in which A is the project area of the cathode. Internal resistance (R_i) was calculated by linear regression of voltage *vs.* current and open circuit voltage (OCV) was the voltage obtained at zero current. The Coulombic efficiency (CE) was calculated from the total current production (Q_{ex}) and the total initial added COD of glucose (equation 3). The chemistry oxygen demand of glucose is 1.063 g/L.

$$CE = \frac{Q_{ex}}{COD_{glucose} \times V \times F \times b \div M} \quad (3)$$

in which V is liquid volume (0.02 L), F is Faraday's constant (96485 C/mol of e^-) and b is mol of e^- produced per mol of O_2 (4 mol/mol), M is the mole mass of O_2 (32 g/mol).

3. RESULTS AND DISCUSSION

Fig. 1 shows the X-ray diffraction patterns for the Pt-Co/G nanoparticles, a commercial Pt/C catalyst and GO. From the previous report [25, 29], the graphite and RGO both exhibited characteristic (0 0 2) diffraction peak at ca. 26.7 º. In this study, upon oxidation/exfoliation of graphite with strong acids, a smaller broader peak at 10.8 º appeared for GO. It indicates the ordering of the graphene layers in graphite was disrupted and the complete oxidation of graphite. For Pt-Co/G, the appearance of the diffraction peak at 23.8 º (due to the 002 reflection) suggests that the GO was reduced by EG [30], thus restoring the crystal structure to that of graphene. It also indicates the Pt-Co alloy was loaded on the graphene. The XRD pattern for Pt-Co/G catalyst is very similar to that for Pt/C, without any obvious additional peaks, four peaks are characteristics of the face-centered-cubic (fcc) crystalline Pt, corresponding to the planes (1 1 1), (2 0 0), (2 2 0) and (3 1 1), respectively. The reflection peaks of the Pt-Co/G samples are shifted to higher angles compared to those of Pt/C, revealing decreased lattice parameters and a high level of alloying [31]. And it indicates the contraction of lattice by the incorporation of Co in the fcc structure of Pt due to alloy formation [32]. The compressed Pt–Pt bond length has been shown to lower the valence band center relative to the Fermi level [33], reduce the binding strength and/or coverage of oxygenated adsorbates, and enhance ORR activity. The Pt/C and Pt-Co/G catalyst particle sizes, calculated from XRD data (2 2 0) peak of the Pt use the Scherrer equation by Jade software, is 3.6 and 4.0 nm, respectively.

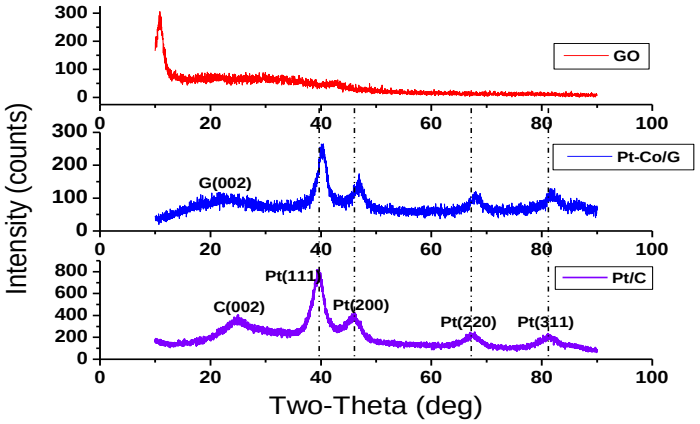

Figure 1. X-ray diffraction patterns for the GO, commercial Pt/C 20% catalyst and Pt-Co/G

Fig. 2 presents a typical TEM image of graphene-supported Pt–Co alloy catalyst with a Pt/Co atomic ratio of 1:1 and its corresponding particle size distribution histogram. As can be observed from the TEM micrograph, the Pt-Co particles appears as small particles, which were well and homogeneously dispersed on the graphene. Good dispersion of metallic nanoparticals could be due to the EG as the reduction agent and stabilizer. The mean particle size was ca. 4.2 nm, which was calculated according to equation 4.

$$d = \frac{\sum_i n_i d_i}{\sum_i n_i} \tag{4}$$

where n_i is the frequency of occurrence of particles with size d_i. The average particle size of Pt-Co catalyst calculated from the TEM image is in good agreement with this measured by the Scherrer equation in the XRD peak.

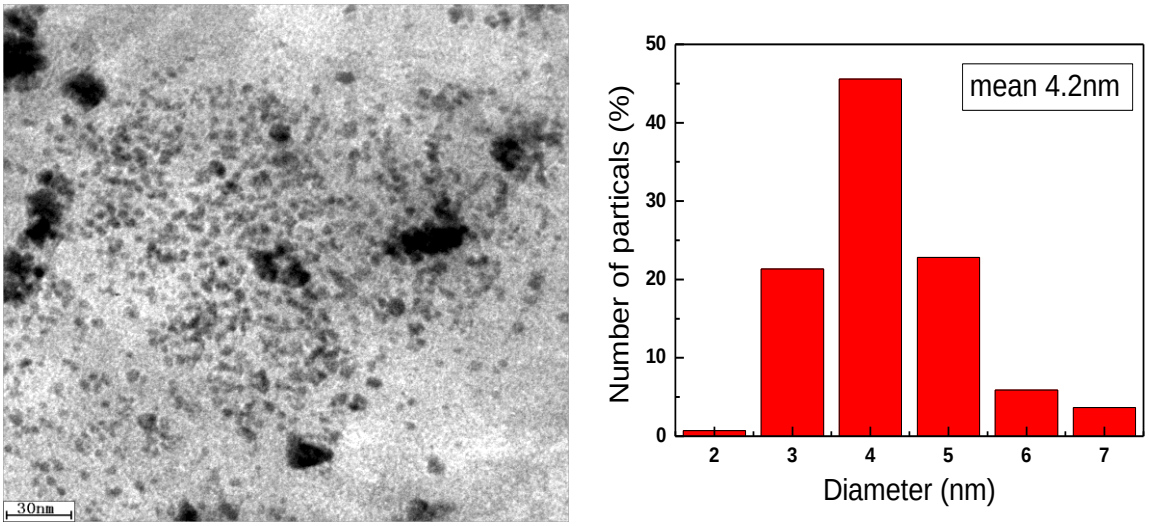

Figure 2. TEM images and histogram of the Pt- Co/G catalysts

The electrochemical performance of catalyst materials is very sensitive to their surface composition and structures. Therefore electrocatalytic activity towards ORR of the as-prepared Pt-Co/G nanoparticles was evaluated by cyclic voltammetry (CV). The measurements were performed in a 0.5 M H_2SO_4 aqueous electrolyte. Fig. 3 shows the cyclic voltammograms of Pt-Co/G catalysts with the scan rate100 mV/s between -0.25V to 1.2V (vs SCE). From the CVs shown in Fig. 3, the hydrogen adsorption/desorption peaks and preoxidation/reduction peaks of the Pt surface on Pt are clearly seen , indicating the presence of polycrystalline Pt for the two kinds of catalyst. The current of the hydrogen region decreases for the Pt-Co/G catalyst, indicative the electrochemical active surface area of Pt-Co/G catalyst is lower than the commercial Pt/C. The real surface area of the Pt was determined from the hydrogen adsorption peaks shown in fig 4. The commonly accepted value is 210 $\mu C \cdot cm^{-2}$ for platinum. The obtained electrochemical active surface area for the Pt/C and Pt–Co bimetallic catalyst is 39.5m^2/g and 34.6 m^2/g, respectively. Meanwhile, The water activation and Pt–OH formation peaks are now clearly discernible in Fig. 3 for the two catalysts. Form Pt-Co/G catalysts the onset of the water activation and Pt–OH formation on alloy surfaces is shifted to higher potentials than it from Pt/C catalyst. A previously suggested kinetic model for the ORR [34] links the delayed formation of Pt–OH

surface layers to a larger number of available surface sites for adsorption of molecular oxygen. A shift in E_{Pt-OH} has therefore been suspected to correlate with increases in the ORR activity [35].

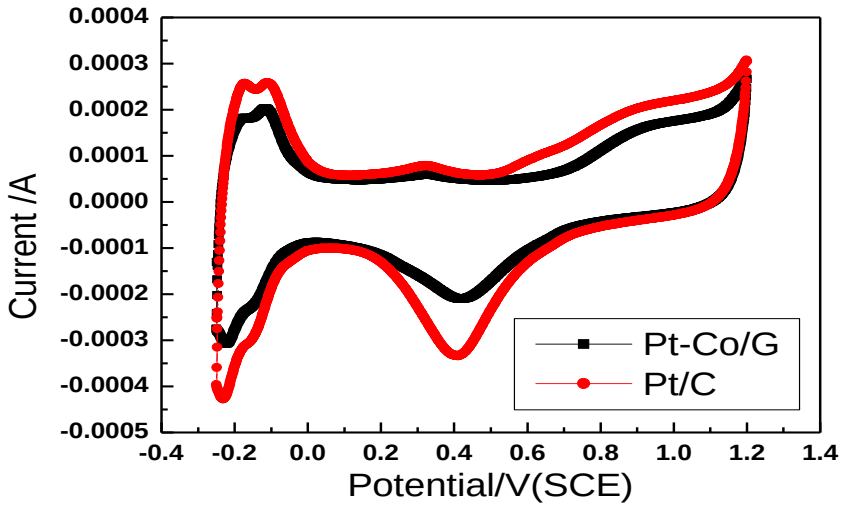

Figure 3. CVs of the Pt–Co/G and Pt/C catalysts in 0.5 M H_2SO_4 at the scan rate of 100 mV/s.

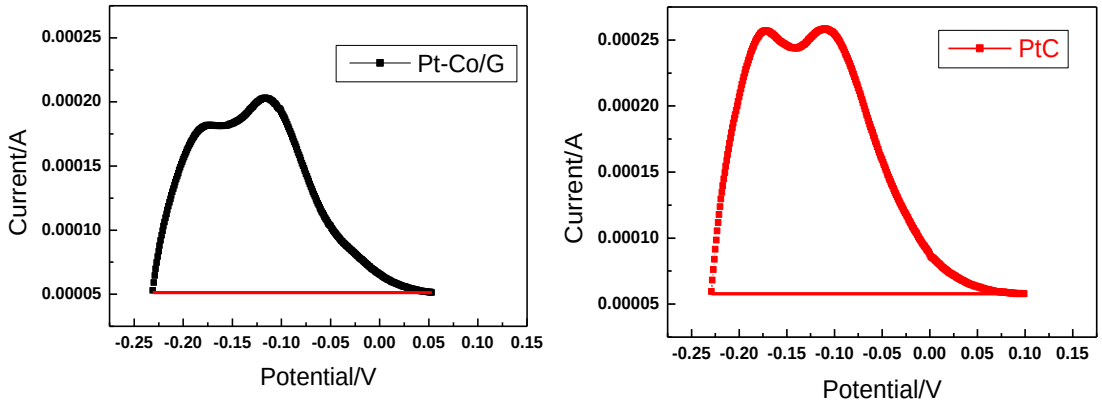

Figure 4. Hydrogen adsorption region of the two catalysts.

In order to evaluate the catalytic active and long-term stability of the catalyst, the cell voltage over a whole operation period were examined in single-chamber MFCs. Electricity generation with 1g/L glucose for Pt/C and Pt-Co/G alloy catalysts was compared in the MFCs (Fig 5A). The maximal output voltage of MFC with the Pt-Co/G ally catalyst is higher than with Pt/C catalysts in the first circle, this indicate the Pt-Co/G ally catalyst has a rather high ORR catalytic active compare with the Pt/C, but in the following circles, the maximal output voltage of MFC with Pt-Co/G is lower and lower than it with Pt/C, it shows that the long-term stability of the catalyst prepared in this study is not good as the commercial Pt/C. In addition, the Coulombic efficiency of the MFC with Pt-Co/G ally catalyst (71.3%) was higher than with Pt/C catalyst (52.0%), which was calculated from the first circle (Fig 5B). Thereby we could conclude that the performance of the Pt-Co/G ally catalyst in the MFC is comparable with the Pt/C catalyst.

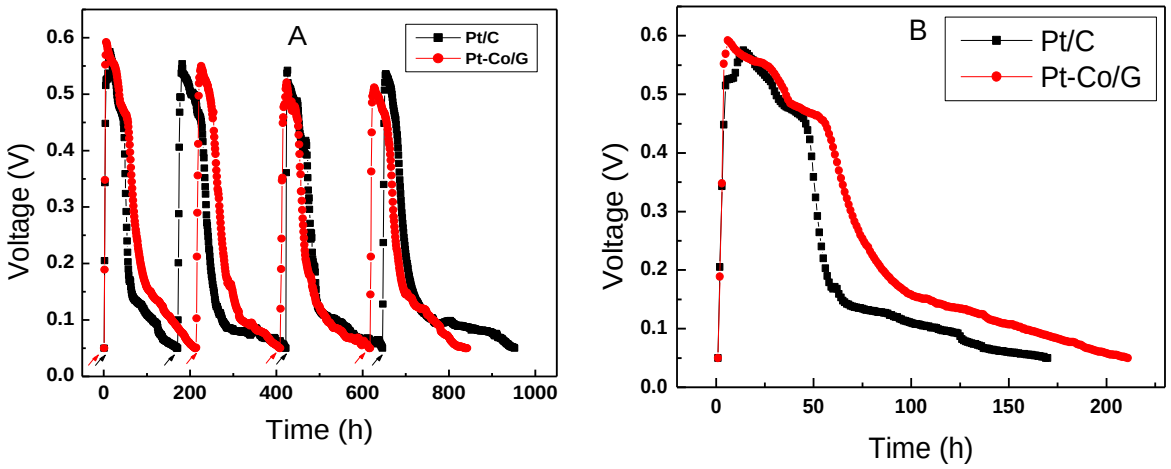

Figure 5. Comparison voltage generations for Pt/C and Pt-Co/G alloy catalysts across a 1000Ω external resistance in air cathode single-chamber MFCs over the long-term operation（A）, the concentration for each substrate was 1 g/L glucose. The arrows indicate the substrate addition. Voltage generations for the first circle (B).

The performances of MFCs with Pt-Co/G and Pt/C cathodes were monitored through gradually decreased external circuit resistances (from 20000 to 20 Ω) to determine power densities and polarization curves for each of the catalyst. The obtained power densities and polarization curves are shown in Fig. 6. The maximum power density of the MFC with a Pt-Co/G cathode was 1378 mW/m^2, which was a little lower than that with a Pt/C cathode (1406 mW/m^2). Internal resistance was estimated from the slope of the plot of voltage versus current, and it was observed to be 178 Ω and 228 Ω in Pt-Co/G cathode and Pt/C cathode MFCs, respectively. The electrochemical reaction rates could be evaluated by the open circuit potential (OCP). A higher OCP value was related to a higher reaction rate [36]. The OCP of the MFC with a Pt-Co/G cathode was 0.71V, which was similar to that with a Pt/C cathode (0.77 ±0.01 V), indicating the ORR rate of the Pt-Co/G catalyst was comparable with the Pt/C catalyst.

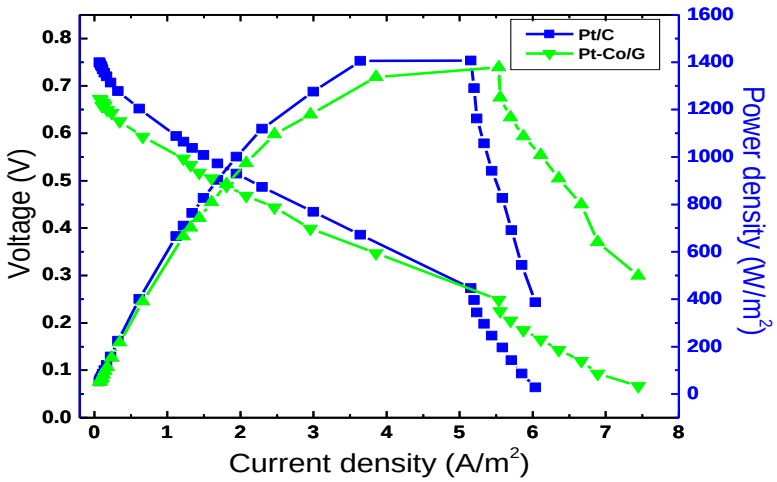

Figure 6. Power density curve and polarization curve for Pt-Co/G ally catalyst (Pt: Co atomic ratio of 1:1; 0.375 mg Pt/cm^2), and Pt/C (0.5 mg Pt/cm^2).

4. CONCLUSIONS

The Pt-Co/G alloy nanoparticles were investigated as replacement for commercial Pt/C as the cathode catalyst in MFCs in this study. Studies with XRD and TEM reveal that Pt-Co/G nanoparticles are approximately 4.1 nm. The electrochemical results demonstrate that the catalytic of the Pt-Co/G possess highly ORR catalyze activity and comparatively stable. The power density of the MFC with a Pt-Co/G cathode was a litter lower than that with a Pt/C cathode, while, the price of a Pt-Co/G catalyst was approximately three-quarter of Pt/C catalyst. The Pt-Co/G catalyst prepared in this study exhibits almost the same catalytic performance to that of Pt/C supporting the established alloying effect. And it clearly suggests that graphene can be an excellent carbon support for high performance ORR catalysts in MFC cathodes. In terms of easy fabrication, lower cost and high power production, Pt-Co/G showed a great potential to be used as a cost-effective catalyst in air cathode of MFCs.

ACKNOWLEDGEMENTS
The work was financially support by the National Natural Science Foundation of China (20906043, 31170110), the promotive research fund for young and middle-aged scientists of Shandong Province (2009BSB01453), the Natural Science Foundation of Shandong province (ZR2010BQ009, ZR2011EL002) and the Taishan Scholarship of Shandong Province.

References

1. D. Pant, G. V. Bogaert, L. Diels, K. Vanbroekhoven, *Bioresource. Technol*, 101 (2010) 1533–1543
2. J. D. Aiken, R. G. Finke, J. Mol.*Catal. A*, 145 (1999) 1–44
3. R. S. Ingram, R. W. Murray, *Langmuir*, 14 (1998) 4115–4121
4. C. J. Zhong, J. Luo, B. Fang, B. N. Wanjala, P. N. Njoki, R. Loukrakpam, J. Yin, *Nanotechnology*，21 (2010) 062001
5. J.B. Joo, Y.J. Kim, W.Y Kim, N.D. Kim, P. Kim, Y.G. Kim, Y.W. Lee and J. Yi, *Korean J. Chem. Eng.*, 25 (2008) 431-436
6. Y.W. Ma, Z.R. Liu, B.L Wang, L. Zhu, J.P. Yang, X.G. Li, *New. Carbon. Mater*., 27 (2012) 250-257
7. J.R. Kim, J.Y. Kim, S.B. Han, K.W. Park, G.D. Saratale, S.E. Oh, *Bioresource Technol*., 102 (2011) 342–347
8. L.X. Ding, A.L. Wang, G.R.. Li, Z.Q. Liu, W.X. Zhao, C.Y. Su and Y.X. Tong, *J. Am. Chem. Soc.*, 134 (13) (2012) 5730–5733
9. S. Maass, F. Finsterwalder, G. Frank, R. Hartmann, C. Merten, *J Power Sources*, 176 (2008) 444–51
10. A.K. Geim, K.S. Novoselov, *Nat Mater*, 6 (2007)183–91
11. B. Seger, P.V. Kamat, *J. Phys. Chem. Lett*., 113 (2009) 7990–7995
12. W. Gao, L.B. Alemany, L. Ci, P.M. Ajayan, *Nat. Chem*., 1 (2009) 403–8
13. S. J. Wang, Y. Geng, Q.B. Zheng, J. K. Kim, *Carbon*, 48 (2010) 1815–1823
14. S. Guo, S. J. Sun, *Am. Chem. Soc*., 134 (2012) 4
15. Y. Liang, Y. Li, H. Wang, J. Zhou, J. Wang, T. Regier, H. Dai, *Nat. Mater*, 10 (2011) 780.
16. C. V. Rao, A. L. M. Reddy, Y. Ishikawa, P. M. Ajayan, *Carbon*, 49 (2011) 931
17. Y.X. Xu, H. Bai, G.W. Lu, C. Li, G.Q. Shi, *J. Am. Chem. Soc.*, 130 (18) (2008) 5856–5857
18. S. Guo, S. Dong, E. Wang, *ACS. Nano*, 4 (2010) 547−555
19. R. Kou, Y. Shao, D. Mei, Z. Nie, D. Wang, C. Wang, V. Viswanathan, S. Park, I. A. Aksay, Y. Lin, Y. Wang, J. Liu, *J. Am. Chem. Soc.*, 133 (2011) 2541 − 2547.

20. X. Chen, G. Wu, J. Chen, X. Chen, Z. Xie, X. Wang, *J. Am. Chem. Soc*., 133 (2011) 3693−3695
21. Y. Liang, Y. Li, H. Wang, J. Zhou, J. Wang, T. Regier, H. Dai, *Nat. Mater*., 10 (2011) 780−786
22. Y. Li, H. Wang, L. Xie, Y. Liang, G. Hong, H. Dai, *J. Am.Chem. Soc*., 133 (2011) 7296−7299
23. J.W. Hummers, R.E. Offeman, *J. Am. Chem. Soc*., 80 (1958)1339
24. S. Stankovich, D.A. Dikin, G.H.B. Dommett, K.M. Kohlhaas, E.J. Zimney, E.A. Stach, R.D. Piner, S.T. Nguyen, R.S. Ruoff, *Nature*, 442 (2006) 282-286.
25. C. V. Rao, A. L.M. Reddy, Y. Ishikawa , P. M. Ajayan, *Carbon*, 49 (2011）931-936
26. D. R. Lovley, E. J. Phillips, *Appl. Environ. Microb.*, 54 (1988) 1472-1480
27. J.R. Kim, J.Y . Kim, S.B. Han, K.W. Park, G.D. Saratale, S.E. Oh, *Bioresource. Technol*., 102 (2011) 342–347
28. B.E. Warren, X-ray Diffraction, Addison-Wesley, Reading, MA, (1969)
29. W. He, H.J. Jiang, Y. Zhou, S.D. Yang, X.Z. Xue, Z.Q. Zou, X.G. Zhang, D.L. Akins, H.Yang, *Carbon*, 50 (2012) 265-247
30. C. Xu, X. Wang, J.W. Zhu, *J. Phys. Chem. C*, 112 (50) (2008) 19841–19845
31. C. Lee, H. Chiou, S. Wu, C. Wu, *Electrochim. Acta*, 56 (2) (2010) 687–92
32. R.C. Venkateswara, B. Viswanathan, *J. Phys. Chem. C* , 113 (2009) 18907–18913
33. L. Grabow, Y. Xu, M. Mavrikakis, *Phys. Chem. Chem. Phys*., 8 (2006) 3369–74.
34. U.A. Paulus, A. Wokaun, G.G. Scherer, T.J. Schmidt, V. Stamenkovic, V. Radmilovic, N.M. Markovic, P.N. Ross, *J. Phys. Chem. B*， 106 (2002) 4181.
35. S. Koh, M. F. Toney, P. Strasser, *Electrochim. Acta*, 52 (2007) 2765–2774
36. D.R. Lovley, *Curr. Opin. Biotech.*, 19 (2008) 564